

CrossMark  
click for updates

Cite this: DOI: 10.1039/c6ta07086h

# Photon energy storage materials with high energy densities based on diacetylene–azobenzene derivatives†

Ggoch Ddeul Han,<sup>a</sup> Sarah S. Park,<sup>b</sup> Yun Liu,<sup>a</sup> David Zhitomirsky,<sup>a</sup> Eugene Cho,<sup>a</sup> Mircea Dincă<sup>b</sup> and Jeffrey C. Grossman<sup>\*a</sup>

Photocontrolled self-assembly of molecules has been utilized to change the physical properties of organic materials for various applications, while photon energy storage materials that incorporate photochromic molecules such as azobenzenes have been recognized as another highly attractive class of materials that convert and store photon energy in the strained chemical bonds. Herein, we demonstrate the photocontrolled self-assembly and disassembly of photon energy storage materials based on new diacetylene derivatives with azobenzene moieties and with varied alkyl spacers and linkers. We developed a series of symmetric diacetylenes and polydiacetylenes and obtained high energy-density materials that can store up to 176.2 kJ mol<sup>-1</sup> (or 200.2 kJ mol<sup>-1</sup>, if completely charged); more than double that of pristine azobenzene. The extra energy storage in the materials in addition to the isomerization enthalpy of azobenzene units is enabled by the different phase of materials in the ground state (crystalline solid) and in metastable state (amorphous solid/liquid). It is notable that the phase change characteristic of organic materials can be a parameter to consider in terms of designing high energy density photon energy storage materials.

Received 17th August 2016  
Accepted 12th September 2016

DOI: 10.1039/c6ta07086h

www.rsc.org/MaterialsA

## Introduction

Solar energy harvesting and conversion into other forms of energy (*i.e.* electricity, chemical fuels, and heat) have been a focus of research efforts for efficient and renewable energy utilization. Various types of solar cells incorporate inorganic,<sup>1</sup> organic,<sup>2</sup> and hybrid materials,<sup>3,4</sup> systems for photocatalytic fuel generations<sup>5,6</sup> employ wide-band metal oxides, and solar thermal collection and storage largely depend on fluids such as water, air, molten salts, and phase-change (PC) materials.<sup>7</sup> Particularly, materials with high PC enthalpy have great potential to store solar heat. Another less known but highly

attractive method to convert and store solar energy in the form of heat is to incorporate photochromic molecules, referred to as photon energy storage materials, which can isomerize to metastable forms upon filtered solar irradiation, store photon energy in the strained chemical bonds, and release the stored energy as heat upon reverse isomerization. These materials possess unique advantages such as off-grid energy storage and triggered energy release compared to other solar devices and PC materials, and thus the facile fabrication and operation of the systems can be exploited for large-scale and portable applications where on-demand release of heat is necessary. The enthalpy difference of the metastable and thermodynamically stable states,  $\Delta H$ , is the conformational energy stored in the materials, which may be triggered to release by optical, thermal, electrical, and electrochemical methods.<sup>8</sup> There are various photochromic molecules that exhibit reversible structural changes upon illumination, notably anthracene,<sup>9</sup> stilbene,<sup>10</sup> fulvalene diruthenium,<sup>11</sup> azobenzene,<sup>12</sup> and norbornadiene<sup>13</sup> systems. Among these candidates, azobenzene derivatives are selected for our study due to their low cost, facile synthesis, and remarkable chemical stability over repeated operation of photoisomerization and reverse thermal isomerization between *trans* and *cis* forms.

One of the important properties to improve in the azobenzene systems is the energy storage capacity, *i.e.*  $\Delta H$  (41.4 kJ mol<sup>-1</sup> for pristine azobenzene).<sup>14</sup> Therefore, strategies to increase the energy storage in azobenzene derivatives have been

<sup>a</sup>Department of Materials Science and Engineering, Massachusetts Institute of Technology, 77 Massachusetts Avenue, Cambridge, MA, 02139, USA. E-mail: jcg@mit.edu

<sup>b</sup>Department of Chemistry, Massachusetts Institute of Technology, 77 Massachusetts Avenue, Cambridge, MA, 02139, USA

† Electronic supplementary information (ESI) available: Synthetic procedures for compounds 1–8 and polydiacetylenes, a detailed description on the structures of compounds 5–8, packing structures of compound 3, simulated structures of polymer 3, thermochromism of polymer 3, UV-vis absorption spectra of compounds 1–8 during charging or discharging, DSC cycles of charged compound 1, kinetic studies on thermal reverse isomerization and  $t_{0.5}$  of compounds 3–4, PXRD patterns of compounds 1–8 and polymers 1–4, TGA plots of compounds 1–4, <sup>1</sup>H and <sup>13</sup>C NMR spectra of compounds 1–8, and X-ray experimental details of compound 3. CCDC 1499609. For ESI and crystallographic data in CIF or other electronic format see DOI: 10.1039/c6ta07086h

investigated by both computation and experiments, with one effective method shown to be the anchoring of photochromic molecules to rigid templates such as carbon nanotubes, graphene, and other hydrocarbons,<sup>15–20</sup> which takes advantage of the relative strength of intermolecular interactions in the close-packed *trans* and *cis* isomers. Even without the templates, we expect that the intermolecular interactions such as H-bonding, van der Waals force, and  $\pi$ – $\pi$  interaction can significantly influence the photon energy storage density. The photo-switching *vs.* packing density and alignment of azobenzene materials has been explored for some macrocyclic<sup>21–23</sup> and linear<sup>24</sup> azobenzene derivatives, particularly for liquid crystalline materials, for applications in photolithography and actuation. The collective change of the intermolecular interactions in such materials can be observed as a macroscopic solid–liquid phase transition. Despite the outstanding progress towards modifying both the molecular *trans*–*cis* transition for individual or polymerized azobenzene derivatives, or for controlling the liquid crystalline order or packing in such materials, the combination of the two effects has yet to be demonstrated in a broad set of organic molecules and polymers as a method for enhancing solar energy storage performance.

In this work, we probe the opportunity for high energy storage in photon energy storage materials realized by different degrees of intermolecular interactions in *trans* and *cis* isomers and suggest azobenzene-containing diacetylene as an effective storage platform, since diacetylenes are easily functionalized and prone to self-assembly, displaying crystalline-like packing due to strong intermolecular interactions. They can also be rapidly photopolymerized by UV illumination to produce polydiacetylenes bearing azobenzene-containing side chains on the rigid conjugated backbones, which resemble the structure of rigid templates decorated with closely-packed photochromic units. Previous efforts on azobenzene-decorated diacetylenes and polydiacetylenes have focused on asymmetric structures where azobenzene groups functionalized on one side and long alkyl chains on the other side are designed to enable the self-assembly of molecules into vesicles and tubes<sup>25</sup> or bilayer films<sup>26,27</sup> for applications such as photocontrolled molecular recognition and reversible optical switch.<sup>28</sup> Building upon the knowledge gained in these studies regarding the structural change of the azobenzene-functionalized diacetylenes, we are able to design symmetric diacetylenes that enable the high loading and ordered arrangement of azobenzene groups. The compact systems of the azobenzene derivatives without bulky groups are desirable to maximize the gravimetric and volumetric energy densities of photon energy storage materials. Herein, we present high energy storage materials based on the azobenzene-functionalized diacetylenes which exhibit up to 113% higher  $\Delta H$  (per azobenzene unit) than that of pristine azobenzene as a result of the strong intermolecular interaction in the ordered *trans* state and the significant loss of the interaction in the *cis* conformation. In order to understand this new type of material design space, we explore the effects of alkyl spacer lengths between the diyne core and terminal azobenzene groups, intermolecular H-bonding, and various groups functionalized on the azobenzene moieties. X-ray diffraction

analysis was conducted to understand the packing and the intermolecular interactions of the materials, and *ab initio* calculations were employed to help shed light on the relative energy storage mechanisms in this series of molecules.

## Experimental

### Materials

Dodeca-5,7-diyneedioic acid and docosa-10,12-diyneedioic acid were purchased from GFS chemicals. Hexadeca-7,9-diyneedioic acid was synthesized following reported procedures.<sup>29,30</sup> Azobenzene precursors were purchased from Sigma-Aldrich and Alfa Aesar. All the compounds purchased from commercial sources were used as received.

### Measurements

<sup>1</sup>H and <sup>13</sup>C NMR spectra were taken on Varian Inova-500 spectrometers. Chemical shifts were reported in ppm and referenced to residual solvent peaks (CD<sub>2</sub>Cl<sub>2</sub>: 5.33 ppm for <sup>1</sup>H, 53.84 ppm for <sup>13</sup>C and DMF-d<sub>7</sub>: 8.03, 2.92, and 2.75 ppm for <sup>1</sup>H, and 163.15, 34.89, and 29.76 ppm for <sup>13</sup>C). A Bruker Daltonics APEXIV 4.7 Tesla Fourier transform ion cyclotron resonance mass spectrometer was used for high-resolution mass determination with an electrospray (ESI) ionization source. Elemental analyses of compounds 1–4 were performed by Robertson Microlit Laboratories (Ledgewood, NJ). UV-vis absorption spectra were recorded using a Cary 5000 UV-vis spectrophotometer in a 10 mm path length quartz cuvette. Thermogravimetric analyses were performed with a Q series TGA Q500 (TA Instruments) under nitrogen to ensure the thermal stability of compounds at high temperatures up to 250 °C. DSC analysis was conducted on a Q series DSC Q10 (TA Instruments). Powder X-ray diffraction (PXRD) patterns were recorded on Bruker D8 Discover diffractometer using Nickel-filtered Cu-K $\alpha$  radiation ( $\lambda = 1.5418 \text{ \AA}$ ) with an accelerating voltage and current of 40 kV and 40 mA, respectively. Samples for PXRD were prepared by placing a thin layer of the appropriate material on a zero-background silicon crystal plate.

### Solvent-assisted charging procedures and the preparation of charged samples for heat release measurements

Powder samples were dispersed in dichloromethane (*ca.* 0.2 mg mL<sup>-1</sup>) by sonication, and were illuminated under a Blak-Ray B-100AP/R (UVP) high intensity UV lamp (365 nm, 100 W) while being stirred (placed 25 cm away from the lamp). The solution samples were kept at room temperature while being charged, and were mostly dissolved in dichloromethane when completely charged. The solutions were then dried under reduced pressure (*ca.* 50 mTorr) in the dark, and the resulting solid or viscous liquid was transferred to a DSC pan for heat release measurements. In order to remove any residual solvent in the uncharged (*trans*) powder samples, the compounds were dried in a vacuum at 100 °C overnight prior to the charging process.

## X-ray diffraction studies

Low-temperature data were collected on a Siemens three-circle diffractometer coupled to a Bruker-APEX CCD detector with graphite-monochromated Mo  $K\alpha$  radiation ( $\lambda = 0.71073 \text{ \AA}$ ), performing  $\phi$ - and  $\omega$ -scans. The structure was solved by direct methods (SHELXS) and refined against  $F^2$  on all data by full-matrix least squares with SHELXL-2015.<sup>31</sup> All non-hydrogen atoms were refined anisotropically. Hydrogen atoms were included in the model at geometrically calculated positions and refined using a riding model.

## Ab initio simulation of the molecular structures

Ab initio relaxation and calculation of the ground-state energy of the molecular structures are performed at the Density Functional Theory (DFT) level with the exchange–correlation energy of the Perdew–Burke–Ernzerhof functional<sup>32</sup> (PBE) using VASP.<sup>33,34</sup> All the molecular structures are relaxed until the forces acting on all the atoms are less than  $0.01 \text{ eV \AA}^{-1}$ . Wave function expansion cuts off at 700 eV to ensure the simulation accuracy. Lattice parameters are allowed to relax during the relaxation of crystal structures. For the simulation of freestanding molecules, we use a vacuum of at least  $10 \text{ \AA}$  in all three directions to avoid self-interaction through the periodic boundary condition.

## Results and discussion

### The structures of symmetric azobenzene-functionalized diacetylenes and polydiacetylenes

In order to understand and develop design principles for enhancing the energy density of self-assembling materials, we first designed and synthesized symmetric diacetylenes with

terminal azobenzene groups to maximize the gravimetric energy density and the volume change of the molecules upon photoisomerization (Fig. 1a). An important design principle was to control the relative strength of intermolecular interactions and the molecular packing dynamics of diacetylene derivatives before and after the photoisomerization of azobenzene units. Based on these ideas, we varied the lengths of alkyl spacers and incorporated two types of linker groups (*i.e.* amide and ester moieties for the presence and absence of intermolecular H-bonding) in the diacetylene structures as shown in Fig. 1a.

Compounds 1–3 are diazobenzenes amide-linked to dodeca-5,7-diyne, hexadeca-7,9-diyne, and docosa-10,12-diyne, respectively. Depending on the length of the alkyl spacer between the diyne core and azobenzene groups, the thermal properties of the compounds change gradually, which indicates the varied strength of intermolecular interactions; for example, compound 1 with the shortest spacer possesses the highest melting point of  $266 \text{ }^\circ\text{C}$ , and compounds 2 and 3 bearing longer spacers exhibit lower melting points of  $233 \text{ }^\circ\text{C}$  and  $213 \text{ }^\circ\text{C}$ , respectively. From this observation, we can infer that the intermolecular H-bonding interaction of amide linkers in compounds 1–3 is weakened as longer alkyl spacers are present due to the steric repulsion of neighboring alkyl chains. Compound 4, docosa-10,12-diyne linked by esters to azobenzene groups, displays the lowest melting point of  $136 \text{ }^\circ\text{C}$ , attributed to the absence of H-bonding linkers. Additionally, compounds 5–8 with various terminal functional groups (electron-donating, electron-withdrawing, and extended aromatic/conjugated groups) were synthesized to modify the optical properties of unsubstituted compounds by controlling the electron density and delocalization on azo groups.

As shown in Fig. 1b, we hypothesize that the structural change of the azobenzene from *trans* to *cis* forms results in a different

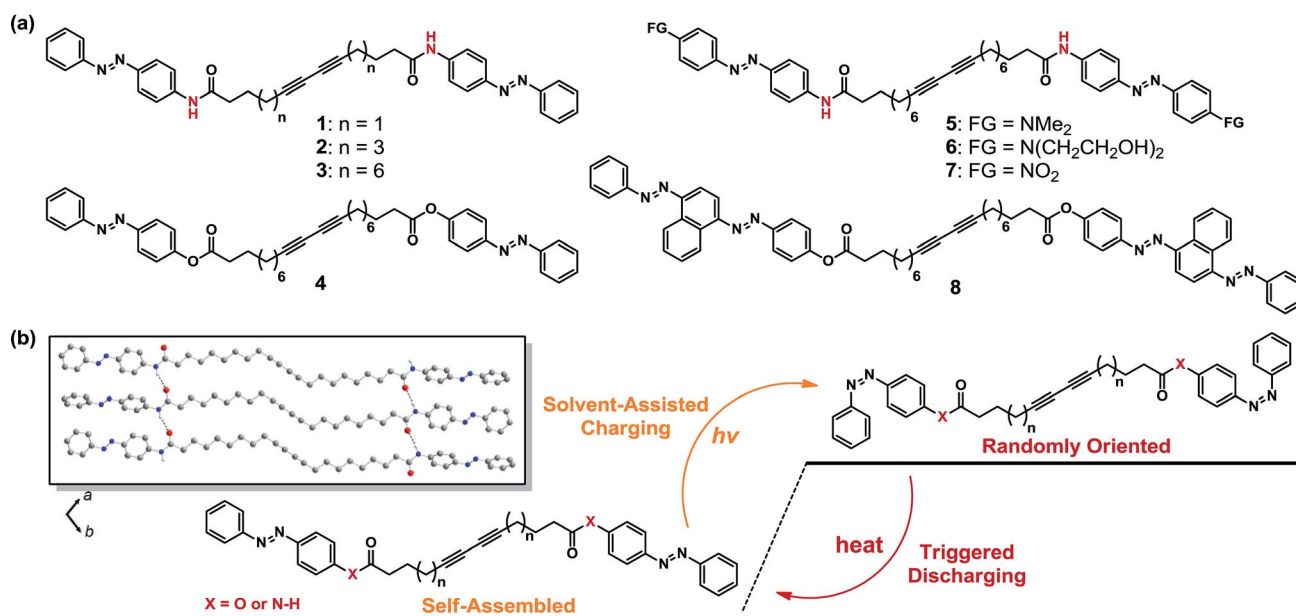


Fig. 1 (a) Azobenzene-functionalized diacetylenes with varying alkyl chain lengths, H-bonding units (marked in red), terminal functional groups, and an extended  $\pi$ -system. (b) A schematic image describing photoisomerization and triggered reverse isomerization of compounds 1–4. The inset shows a crystal structure of compound 3. The dotted lines indicate intermolecular H-bonding. Red, gray, blue and white spheres represent O, C, N and H atoms, respectively. H atoms without hydrogen bonding are omitted for clarity.

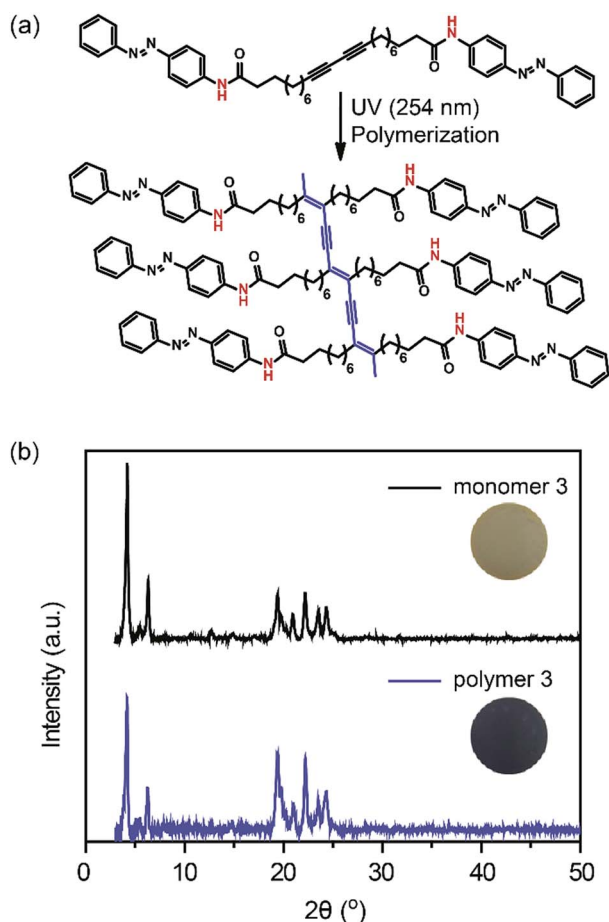


Fig. 2 (a) A schematic photopolymerization of monomer 3 and the structure of polymer 3 with a conjugated backbone. (b) Powder X-ray diffraction patterns and photographs of monomer 3 and polymer 3 in the solid state.

alignment of uncharged and charged diacetylene derivatives. We first obtained a crystal structure of the uncharged compound 3 using single crystal X-ray diffraction analysis as depicted in the inset of Fig. 1b to examine the molecular arrangement. The molecules pack along their long axis, and the neighboring azobenzene groups arrange into herringbone structures. The H-bonding between adjacent amide linkers along the  $b$  axis of the lattice facilitates the packing of molecules as shown. In contrast, intermolecular H-bonding along the  $a$  axis is absent due to the staggered conformation of the adjacent C=O and N-H groups (ESI Fig. S2a†). The powder X-ray diffraction (PXRD) pattern of the as-synthesized compound 3 corresponds well with the diffraction pattern of single crystals (ESI Fig. S2b†), which confirms the structural identity of crystalline powder and single crystals. Atomic structure optimization of the crystal structure of compound 3 monomers at the DFT level also confirms the existence of the H-bonding between the adjacent amide linkers. The cohesive enthalpy of the compound 3 crystal, calculated from the energy difference between the enthalpy of the unit cell with two monomers and the enthalpy of two free-standing monomers, is  $223.0 \text{ kJ mol}^{-1}$ , indicating considerable intermolecular interactions. Since the isomerization of azobenzene requires a free-

volume change of  $120 \text{ \AA}^3$  or more,<sup>35–37</sup> the ordered packing of *trans* isomers will be disrupted and form different molecular arrangements. Due to the non-planar conformation and the increased dipole moment of azobenzene *cis* isomers<sup>38</sup> compared to their *trans* counterparts, the molecules are expected to be randomly oriented, losing a significant degree of intermolecular interactions between the dyne cores, alkyl chains, and aromatic groups.

Polymers of the diacetylene monomers are also crystalline in the ground state, and the syntheses of conjugated polydiacetylenes were easily achieved by UV irradiation (254 nm) of self-assembled azobenzene–diacetylenes in the solid state (Fig. 2a). The yellow-to-blue transition indicates the formation of conjugated backbones (Fig. 2b inserted photographs and Fig. 3a), and the PXRD pattern of the polymer is mostly identical to that of the corresponding monomer, illustrating a negligible or only a small change in the packing of the molecules throughout topochemical photopolymerization.<sup>39</sup> *Ab initio* simulation, however, shows that no intra-molecular H-bonding exists in the same  $b$  axis for the polymer chain of compound 3, due to the larger spatial separation between the N-H and the C=O groups as a result of the structural constraints imposed by the rigid polymer backbone (ESI Fig. S3†).

In this work, we have mainly focused on the high energy storage in the monomers and polymers upon azobenzene isomerization and the release of energy in the form of heat. However, if properly engineered, the azobenzene-functionalized polydiacetylene can be a multifunctional material (*i.e.* a photon energy storage material and a colorimetric indicator of the storage) as the photoisomerization of azobenzene groups and the consequent steric repulsion between the side chains may control the conjugation length of the polymer backbone reversibly. In fact, polydiacetylenes generally exhibit colorimetric transitions (usually from blue to red)<sup>40</sup> upon various stimuli such as heat,<sup>41</sup> mechanical perturbation,<sup>42</sup> and solvents,<sup>43</sup> which shorten the conjugation of the polymer backbones. We also observed the reversible blue  $\leftrightarrow$  red thermochromism of polymer films (ESI Fig. S4†) which indicates their potential to respond to significant steric repulsion between side chains. The development of photochromic materials based on polydiacetylenes that exhibit clear color changes over charging and discharging is an ongoing effort.

### Photon energy storage by photoisomerization and release by thermal reverse isomerization

As shown in Fig. 1b, charging (*trans*  $\rightarrow$  *cis*) of diacetylenes and polydiacetylenes was conducted in solution for the facile photoisomerization of azobenzene units in sufficient free volume, since solid-state charging was suppressed within the crystals due to the steric hindrance between close-packed molecules.<sup>44</sup> UV-vis light absorption by the solution of diacetylenes and dispersion of polydiacetylenes were monitored under illumination at 365 nm for photoisomerization (Fig. 3a). Compounds 1–3 bearing amide linkers display an absorption peak at 360 nm assigned to the  $\pi$ - $\pi^*$  transitions and another peak at 445 nm ascribed to the  $n$ - $\pi^*$  transitions (Fig. 3a and S5a–c†). At a photo-stationary state (PSS) with enriched *cis* isomers, the peak at

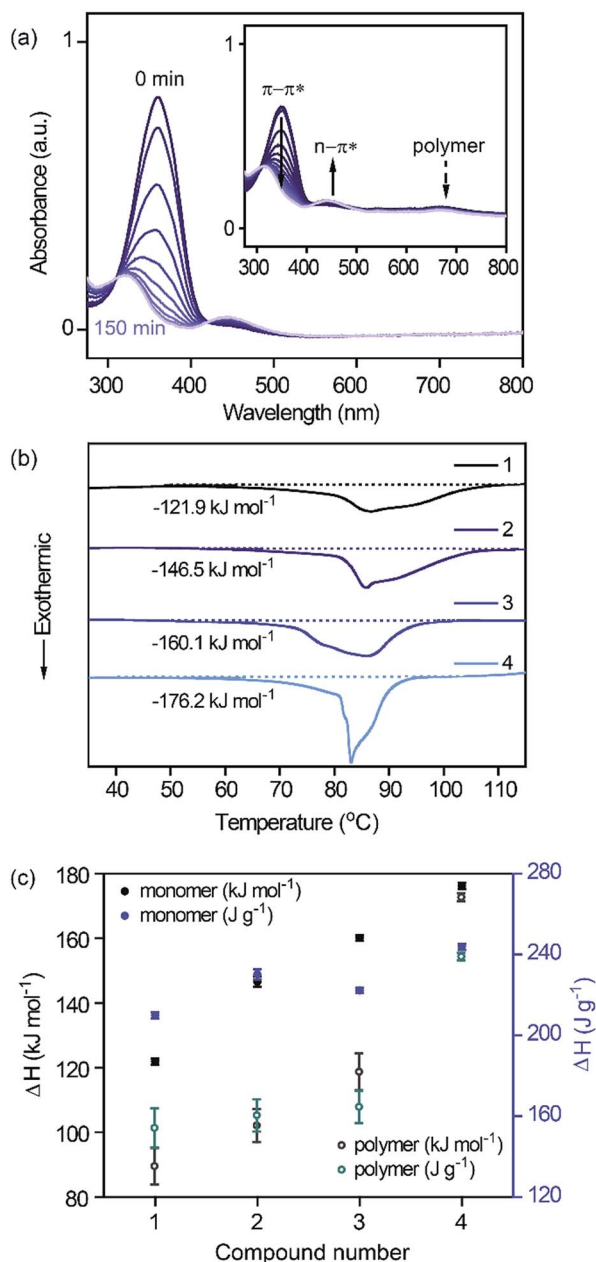


Fig. 3 (a) UV-vis absorption spectra of monomer 3 as it is charged at 365 nm for 150 min. The dark blue line indicates the initial spectrum, and the spectra collected after irradiation are indicated with lighter blue lines. The inset is the absorption spectra of polymer 3. (b) The first DSC traces of monomers 1–4 while temperature increases at 5 °C min<sup>-1</sup> (1–3) and at 2 °C min<sup>-1</sup> (4). The curve areas below the dotted baselines were integrated to calculate the enthalpy changes in the respective compounds. (c)  $\Delta H$  per mole and gravimetric  $\Delta H$  measured for monomers and polymers 1–4.

360 nm blue-shifts toward 325 nm and the one at 445 nm increases up to the highest intensity. Compound 4 with ester linkers shows a  $\pi-\pi^*$  transition at 324 nm and  $n-\pi^*$  transition at 437 nm that are farther apart on the spectra compared to those of the amide derivatives (*i.e.* a less overlap between absorptions induced by those transitions) (Fig. S5d†). On the

Table 1 Heat release of monomers 1–4 measured by DSC

Compound	1	2	3	4
$\Delta H$ [kJ mol <sup>-1</sup> ]	121.9 ± 0.9	146.5 ± 1.6	160.1 ± 0.9	176.2 ± 1.0
$\Delta H$ [J g <sup>-1</sup> ]	209.9 ± 1.6	230.1 ± 2.5	222.1 ± 1.3	243.7 ± 1.4

other hand, compounds 5–8 with terminal functional groups exhibit red-shifted light absorption and a large overlap between the  $\pi-\pi^*$  and  $n-\pi^*$  transitions, hence limiting the selective excitation of the  $\pi-\pi^*$  transition, undergo simultaneous conversion between *trans* and *cis* isomers even by narrow-range light absorption (Fig. S5e–h†). Therefore, compounds 5–8 were charged with very low yields, and the heat release of the charged materials was negligible. This result indicates the importance of designing photoisomer pairs that have the least overlap between the absorption spectrum of each isomer for photon energy storage applications. The absorption characteristics of polymers 1–4 synthesized from the corresponding diacetylene monomers 1–4 consist of the typical  $\pi-\pi^*$  and  $n-\pi^*$  transitions of monomers and additional absorbance at 650–700 nm by conjugated polymer backbones which do not limit the absorption of the photochromic units (inset of Fig. 3a).

The charged solutions were concentrated and dried in the dark, and  $\Delta H$  from reverse thermal isomerization was measured by differential scanning calorimetry (DSC). The first DSC traces of compounds 1–4 in the heating process are shown in Fig. 3b where integration of the exothermic peak corresponds to the energy stored in the *cis* isomer. Complete thermal reversion of the *cis* state to the *trans* state is achieved within the temperature range of measurements, as confirmed by the following cooling scan and the subsequent DSC runs which do not exhibit any endothermic or exothermic feature (Fig. S6†). The  $\Delta H$  of each compound per mole (kJ mol<sup>-1</sup>), and the gravimetric energy density (J g<sup>-1</sup>) are listed in Table 1 and illustrated in Fig. 3c. Among the amide-linked compounds 1–3,  $\Delta H$  per mole (kJ mol<sup>-1</sup>) increases as longer alkyl spacers are used, and it is significantly improved by 47% (1), 77% (2), and 93% (3) per azobenzene unit relative to the  $\Delta H$  of pristine azobenzene (41.4 kJ mol<sup>-1</sup>) even though the molecules are less than 100% charged: about 93% (1), 89% (2), and 93% (3) *cis* at PSS calculated from UV-vis absorbance. If completely charged, compounds 1–3 would exhibit  $\Delta H$  that is 58% (1), 99% (2), and 108% (3) improved per azobenzene unit relative to that of pristine azobenzene. Compound 4 bearing the ester-linked longest alkyl spacers releases the largest energy (176.2 kJ mol<sup>-1</sup>) among the series, which is improved by 113% compared to that of pristine azobenzene, even at a 88% conversion rate. The theoretical  $\Delta H$  of compound 4 is 200.2 kJ mol<sup>-1</sup> that is 142% increased from that of pristine azobenzene. The kinetics of thermal reverse isomerization of compounds 3 and 4 were monitored in solution at varied temperatures (Fig. S7†), and the half-life of each charged compound at 25 °C was 27.8 hours and 98.4 hours, respectively, indicating desirable thermal stability.

Fig. 3c also shows the plots of  $\Delta H$  of polymers 1–4 (Table 2) which are generally lower than the  $\Delta H$  of the monomers (70–98%

Table 2 Heat release of polymers 1–4 measured by DSC

Polymer	1	2	3	4
$\Delta H$ [kJ mol <sup>-1</sup> ]	89.5 ± 5.6	102.1 ± 5.1	118.7 ± 5.7	172.7 ± 1.3
$\Delta H$ [J g <sup>-1</sup> ]	154.1 ± 9.7	160.4 ± 8.0	164.6 ± 8.0	238.9 ± 1.8

of the respective monomer  $\Delta H$ ). The charging and heat release of polymers were not as consistent over multiple trials, unlike the highly reproducible process of monomers (small deviations as shown in Table 1), which may be attributed to the polydispersity of polymer chains. Photopolymerization of self-assembled monomers in films can easily lead to the inhomogeneity of polymer/oligomer/monomer contents in the samples, even if the light exposure is carefully repeated to induce polymerization evenly throughout the entire batch. Depending on the relative monomer and polymer content in the samples, the conversion and  $\Delta H$  can vary. Due to these variations, the standard deviations of the measured  $\Delta H$  values of polymers are larger (Table 2) compared to those of monomers. Lower photon energy storage in polymers compared to monomers has also been recently reported by Zhitomirsky, *et al.* for azobenzene-functionalized PMMA structures.<sup>45</sup> We assume that the polymer aggregation in the dispersion hinders light absorption by the materials, limiting the conversion of azobenzene side chains. However, the trend of  $\Delta H$  per mole (kJ mol<sup>-1</sup>) with the length of alkyl chains among polymers 1–3 is similar to that among monomers 1–3, and the  $\Delta H$  of polymer 4 decreases only slightly relative to that of monomer 4. Also, charged polymers still release larger  $\Delta H$  than pristine azobenzene, increased by 8% (1), 23% (2), 43% (3), and 109% (4). Moreover, the instant polymerization process and the colorimetric behavior of polydiacetylene, compared to other types of polymers, make it an attractive candidate to be a colorimetric material as aforementioned.

It is surprising that all the monomers and polymers in the series exhibit larger  $\Delta H$  than that of pristine azobenzene and that monomer and polymer 4 in particular store more than double the  $\Delta H$  per azobenzene unit. We hypothesize that the additional energy storage would result from different intermolecular interactions in *trans* and *cis* states that enlarge the enthalpy gap between those. As seen in the crystal structures and PXRD, the strong self-assembly of molecules with *trans* azobenzene groups would stabilize the energy of the ground state, and the fact that solid-state charging was not realized in the set of molecules indicates a considerable energy barrier for the azobenzene conversion in the close-packed structures. The charged molecules with metastable *cis* azobenzenes obtained from UV irradiation in solution are likely to be randomly oriented due to the steric repulsion between non-planar azobenzene units, possessing higher enthalpy.

### The impact of phase change of charged materials on energy storage

In order to understand the energy barrier for charging in the solid state and the relative intermolecular interactions in the charged and uncharged materials, we examined the crystallinity

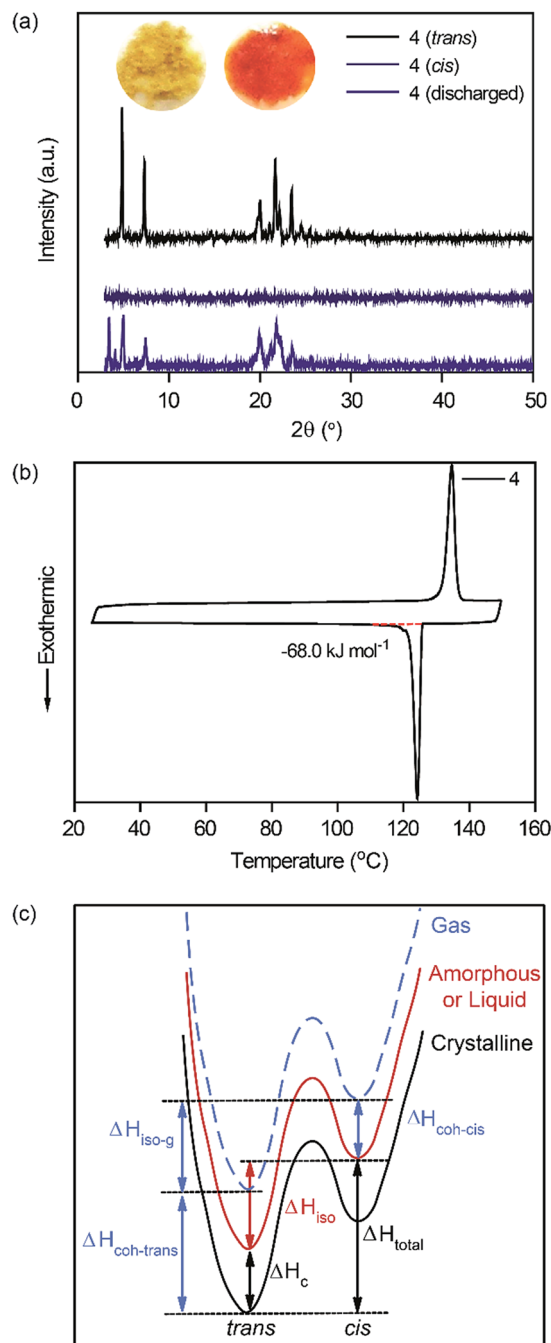


Fig. 4 (a) Powder X-ray diffraction of monomer 4 as synthesized (*trans*), charged (*cis*), and discharged (*trans*). The inset shows photographs of the as-synthesized (left) and charged (right) isomers with different phases (crystalline solid and liquid). (b) A DSC curve of uncharged monomer 4, showing melting and crystallization. The crystallization energy was obtained by integrating the crystallization peak below the dotted red baseline. (c) Energy diagram of azobenzene-derivative isomers (*trans* and *cis*) in different phases (gas, crystalline, amorphous or liquid). The meaning of  $\Delta H_{\text{iso-g}}$ ,  $\Delta H_{\text{c}}$ ,  $\Delta H_{\text{coh-trans}}$ ,  $\Delta H_{\text{coh-cis}}$ ,  $\Delta H_{\text{iso-g}}$ , and  $\Delta H_{\text{total}}$  are explained in the main text.

of compounds before/after charging and after discharging (Fig. 4a). The as-synthesized (uncharged) compounds, both monomers and polymers, are crystalline as sharp peaks are observed by PXRD (additional ESI Fig. S8 and S9†). The charged

**Table 3** The crystallization energy ( $\Delta H_c$ ) of compounds 2–4 measured by DSC<sup>a</sup>

Compound	1	2	3	4
$\Delta H_c$ [kJ mol <sup>-1</sup> ]	N.A.	38.6	58.9	68.0
$\Delta H_c$ [J g <sup>-1</sup> ]	N.A.	60.6	81.7	94.1

<sup>a</sup> Compound 1 was decomposed at a high melting point. The temperature scan rate was 5 °C min<sup>-1</sup> (compounds 2–3) or 2 °C min<sup>-1</sup> (compound 4), identical to the scanning condition for  $\Delta H_{\text{total}}$  measurements.

compounds were found to lose crystallinity, as the absence of diffraction indicates, and the crystallinity is restored when they were discharged (by heat or ambient light). By observing the PXRD patterns and the phase of materials, we find that charged monomers and polymers 1–3 are amorphous solids that undergo phase transition to crystalline *trans* isomers when triggered at a heating rate ranging between 0.5 and 10 °C min<sup>-1</sup>. Charged monomer and polymer 4 are in the viscous liquid state (shown as the inset of Fig. 4a) and discharged at a slower heating rate ranging between 0.5 and 2 °C min<sup>-1</sup> to release the maximum energy. If triggered at a higher scan rate of 5 °C min<sup>-1</sup> or 10 °C min<sup>-1</sup>, compound 4 released 140 kJ mol<sup>-1</sup>, 79% of the maximum capacity, indicating that crystallization of 4 upon thermal isomerization in the liquid is a slower process than that of 1–3. This implies that measured exothermicity is a combined product of azobenzene isomerization and crystallization, and that one could decouple the two phenomena by varying the rate of heating (discharging).

Comparing the relative  $\Delta H$  values among the molecules, we can infer that the length of alkyl spacers and the presence of the H-bonding moiety significantly affect the enthalpy and phase of the metastable state. To estimate the enthalpy difference between the *trans* and *cis* states, originating solely from the relative degree of intermolecular interaction, we measured the crystallization energy ( $\Delta H_c$ ) of each compound using DSC by integrating the crystallization peak (as shown in Fig. 4b with compound 4) for the phase transition of the liquefied *trans* isomer to the solid state. Although the phase transition occurring over the thermal reverse isomerization is not identical to that of the crystallization process from the liquid state (as shown in Fig. S8†), the transition from the randomly oriented amorphous morphology to crystalline packing is similar in both phenomena.

We find that the relative intensity of  $\Delta H_c$  scales with the  $\Delta H_{\text{total}}$  measured experimentally (Tables 1 and 3);  $\Delta H_c$  of compounds 2–4 are 38.6 kJ mol<sup>-1</sup>, 58.9 kJ mol<sup>-1</sup>, and 68.0 kJ mol<sup>-1</sup>, respectively. Thus, it is inferred that intermolecular H-bonding in these molecules lowers the energy gap between the ground and metastable states and that longer alkyl chains weakening the H-bonding are beneficial for large energy storage in this class of materials.

Also, we can suggest that enthalpy associated with the relative degree of intermolecular interactions or the phase of materials contributes to increasing  $\Delta H_{\text{total}}$  and that the high energy storage measured for azobenzene-functionalized

diacetylenes and polydiacetylenes is strongly linked to the high crystallinity of the materials in the ground state and the amorphous or liquid phase of the metastable state. However, this class of materials has higher  $\Delta H$  than pristine azobenzene, even without considering the phase change effect;  $\Delta H_{\text{total}} - \Delta H_c$  per azobenzene unit is 54.0 kJ mol<sup>-1</sup> (2), 50.6 kJ mol<sup>-1</sup> (3), and 54.1 kJ mol<sup>-1</sup> (4), generally improved from the pristine azobenzene by 22–31%.

Fig. 4c shows a new energy diagram of photon energy storage materials that undergo phase change by isomerization of photoswitches (azobenzene in this series of materials).  $\Delta H_{\text{iso}}$  is the isomerization energy of compounds in the amorphous solid or liquid state, and  $\Delta H_c$  is the crystallization energy of the *trans* isomer from either the amorphous solid or liquid state to the crystalline solid.  $\Delta H_{\text{coh-trans}}$  is the cohesive enthalpy of the *trans* isomer from the gas state to the crystalline solid, while  $\Delta H_{\text{coh-cis}}$  is the cohesive enthalpy of the *cis* isomer from the gas state to the amorphous solid or liquid state.  $\Delta H_{\text{iso-g}}$  is the thermal isomerization enthalpy of the charged isomer in the gas phase.  $\Delta H_{\text{total}}$  which is the experimentally measured heat release from the charged materials, can be expressed as the sum of  $\Delta H_{\text{iso}}$  and  $\Delta H_c$ .

To help fully understand this new diagram, we take compound 3 as an example and calculate all relevant thermodynamic quantities using DFT. We find that  $\Delta H_{\text{iso-g}} = 119.0$  kJ mol<sup>-1</sup> from our *ab initio* simulations, and as mentioned previously,  $\Delta H_{\text{coh-trans}}$  computed as the energy difference between the enthalpy of the unit cell with two monomers and the enthalpy of two free-standing monomers, is 112.0 kJ mol<sup>-1</sup>. Using the experimentally measured  $\Delta H_{\text{total}}$  of 160.1 kJ mol<sup>-1</sup>, we calculate  $\Delta H_{\text{coh-cis}}$  according to the diagram as  $\Delta H_{\text{coh-cis}} = \Delta H_{\text{coh-trans}} + \Delta H_{\text{iso-g}} - \Delta H_{\text{total}} = 70.9$  kJ mol<sup>-1</sup>, which corresponds physically to the heat required to evaporate the *cis* monomers from their liquid state. Furthermore, if we assume that the isomerization enthalpy in the liquid state ( $\Delta H_{\text{iso}}$ ) is approximately the same as the isomerization enthalpy in the gas state ( $\Delta H_{\text{iso-g}}$ ), we can predict the crystallization enthalpy ( $\Delta H_c$ ) from this diagram using  $\Delta H_c = \Delta H_{\text{total}} - \Delta H_{\text{iso}} = \Delta H_{\text{total}} - \Delta H_{\text{iso-g}} = 41.1$  kJ mol<sup>-1</sup>. This assumption holds when the strength of intermolecular interactions in the liquid state is the same for both *trans* and *cis* isomers. Since the experimentally measured  $\Delta H_c$  for compound 3 (58.9 kJ mol<sup>-1</sup>) is higher than the calculated  $\Delta H_c$ , this discrepancy suggests that the interaction between the *trans* isomers may be weaker than the *cis* isomers in the liquid state, as a result of the lower polarity of the *trans* compared to that of the *cis*.

Based on the understanding gained from the systematic analysis of the series of molecules in this work, we suggest the following design principle for high energy storage azobenzene-based molecules: *trans* isomers should be self-assembling structures to form crystalline materials, and *cis* isomers need to become liquid by steric distortion in the absence of strong intermolecular interactions such as H-bonding. Molecules with high crystallization energy should be well-suited for the design of high energy density materials. The recently reported work on the azobenzene-functionalized ionic crystal and ionic liquid pair by Kimizuka and coworkers<sup>46</sup> also shows enhanced energy

storage in the systems by photoinduced direct phase transition of materials (without the need of the solvation process). Although the solid-state charging was realized for the ionic liquid, which is desirable for practical applications, the gravimetric energy density ( $143.3 \text{ J g}^{-1}$  for the best molecule) is decreased significantly compared to that of the pristine azobenzene ( $227.3 \text{ J g}^{-1}$ ), due to bulky oligo(ethylene oxide)-based ammonium groups, necessary for lowering the melting point of ionic crystals.

In contrast, azobenzene-functionalized diacetylene and polydiacetylene derivatives reported in this work exhibit comparable or higher gravimetric  $\Delta H$  ( $243.7 \text{ J g}^{-1}$  for compound **4**), although this high energy is only achieved by charging in solution and deposition of dried materials. Although if one were to think of this as a device it would represent only a half-cycle, the goal of this work is not to explore the applications of photon energy storage materials but rather to understand key aspects of the chemistry that could allow us to further increase the energy density by combining macroscopic and molecular-level phase changes. Our results suggest a broad set of design strategies that could enable further development, optimization, and application of this new class of materials. For example, the limitation of the current system could be overcome by attaching bulky functional groups that provide sufficient free volume required for azobenzene photoisomerization in the solid state, despite the potential loss of crystallization enthalpy and the reduced gravimetric energy density. The search for photon energy storage systems that can both store high energy and change the phase in the solid state requires a systematic optimization of the molecular structures by varying the relative degree of intermolecular interactions in the ground and metastable states.

## Conclusions

We present a new series of azobenzene-functionalized symmetric diacetylenes and polydiacetylenes, high energy density photon energy storage materials that can store up to  $176.2 \text{ kJ mol}^{-1}$  (or  $200.2 \text{ kJ mol}^{-1}$ , if completely charged); more than double that of pristine azobenzene, per azobenzene unit. The high energy storage is enabled by the photoisomerization of azobenzene units as well as the change in the intermolecular interactions in *trans* and *cis* states. We believe that the strong self-assembly and close-packed crystalline structure of diacetylene molecules in the ground state is essential to maximize the energy difference from the randomly oriented molecules in the metastable state. Although the charging of such materials in the solid state remains a challenge, due to the suppressed photoswitching in the close-packed structure, further investigation on optimizing the balance between high crystallinity and capability to switch in films will be able to resolve this limitation.

Furthermore, we view this class of materials as a hybrid of traditional organic phase-change (PC) materials and photochromic molecules that can harvest photon energy and store latent heat as well. These hybrid materials offer the potential of new functionality to traditional organic PC materials such as

paraffins and fatty acids, which possess large heats of fusion (around  $150\text{--}250 \text{ J g}^{-1}$ ), and could enable long-term storage of the latent heat at room temperature due to the energy barrier for the reverse isomerization of the photoswitches. Given a broad parameter space of photoswitches and organic-based PC materials, and our newly engineering levers over controlling the *trans* and *cis* phases, this new paradigm in photon energy storage material design will enable a rapid progress in achieving higher energy density and novel functional materials. This approach stands to fully exploit the tremendous potential of these materials for renewable energy storage and heat release applications.

## Acknowledgements

Materials and resources funding for this project were provided by Bavarian Motor Works (BMW, Award No. 4500264959). D. Z. acknowledges his Natural Sciences and Engineering Research Council of Canada Banting Fellowship. Work in the Dinca lab was supported by the U.S. Department of Energy, Office of Science, Office of Basic Energy Sciences (U.S. DOE-BES, Award No. DE-SC0006937). S. S. P. is partially supported by a NSF GRFP (Award No. 1122374). The authors acknowledge access to Shared Experimental Facilities provided by the MIT Center for Materials Science Engineering. We thank Prof. Timothy M. Swager in the Department of Chemistry at MIT for the access to DSC measurement in his laboratories. We thank Dr Peter Müller at MIT (Department of Chemistry X-Ray Diffraction Facility) for crystal structure collection. We thank Ms Li Li at MIT DCIF (Department of Chemistry Instrumentation Facility) for high-resolution mass determination. G. D. H. thanks Dr Bora Yoon for her significant advice on polydiacetylene research.

## Notes and references

- 1 S. E. Habas, H. A. S. Platt, M. F. A. M. van Hest and D. S. Ginley, *Chem. Rev.*, 2010, **110**, 6571–6594.
- 2 S. Günes, H. Neugebauer and N. S. Sariciftci, *Chem. Rev.*, 2007, **107**, 1324–1338.
- 3 M. A. Green, A. Ho-Baillie and H. J. Snaith, *Nat. Photonics*, 2014, **8**, 506–514.
- 4 M. Wright and A. Uddin, *Sol. Energy Mater. Sol. Cells*, 2012, **107**, 87–111.
- 5 Y. Ma, X. Wang, Y. Jia, X. Chen, H. Han and C. Li, *Chem. Rev.*, 2014, **114**, 9987–10043.
- 6 P. V. Kamat and J. Bisquert, *J. Phys. Chem. C*, 2013, **117**, 14873–14875.
- 7 A. Sharma, V. V. Tyagi, C. R. Chen and D. Buddhi, *Renewable Sustainable Energy Rev.*, 2009, **13**, 318–345.
- 8 H. M. D. Bandara and S. C. Burdette, *Chem. Soc. Rev.*, 2012, **41**, 1809–1825.
- 9 A. Lennartson, A. Roffey and K. Moth-Poulsen, *Tetrahedron Lett.*, 2015, **56**, 1457–1465.
- 10 K. Börjesson, A. Lennartson and K. Moth-Poulsen, *ACS Sustainable Chem. Eng.*, 2013, **1**, 585–590.

- 11 K. Moth-Poulsen, D. Coso, K. Borjesson, N. Vinokurov, S. K. Meier, A. Majumdar, K. P. C. Vollhardt and R. A. Segalman, *Energy Environ. Sci.*, 2012, **5**, 8534–8537.
- 12 T. J. Kucharski, Y. Tian, S. Akbulatov and R. Boulatov, *Energy Environ. Sci.*, 2011, **4**, 4449–4472.
- 13 M. Kuisma, A. Lundin, K. Moth-Poulsen, P. Hyldgaard and P. Erhart, *ChemSusChem*, 2016, **9**, 1786–1794.
- 14 R. J. Corruccini and E. C. Gilbert, *J. Am. Chem. Soc.*, 1939, **61**, 2925–2927.
- 15 A. M. Kolpak and J. C. Grossman, *J. Chem. Phys.*, 2013, **138**, 034303.
- 16 A. M. Kolpak and J. C. Grossman, *Nano Lett.*, 2011, **11**, 3156–3162.
- 17 T. J. Kucharski, N. Ferralis, A. M. Kolpak, J. O. Zheng, D. G. Nocera and J. C. Grossman, *Nat. Chem.*, 2014, **6**, 441–447.
- 18 Y. Y. Feng, H. P. Liu, W. Luo, E. Z. Liu, N. Q. Zhao, K. Yoshino and W. Feng, *Sci. Rep.*, 2013, **3**, 3260.
- 19 W. Luo, Y. Feng, C. Cao, M. Li, E. Liu, S. Li, C. Qin, W. Hu and W. Feng, *J. Mater. Chem. A*, 2015, **3**, 11787–11795.
- 20 W. Feng, S. Li, M. Li, C. Qin and Y. Feng, *J. Mater. Chem. A*, 2016, **4**, 8020–8028.
- 21 Y. Norikane, Y. Hirai and M. Yoshida, *Chem. Commun.*, 2011, **47**, 1770–1772.
- 22 M. Hoshino, E. Uchida, Y. Norikane, R. Azumi, S. Nozawa, A. Tomita, T. Sato, S.-i. Adachi and S.-y. Koshihara, *J. Am. Chem. Soc.*, 2014, **136**, 9158–9164.
- 23 E. Uchida, K. Sakaki, Y. Nakamura, R. Azumi, Y. Hirai, H. Akiyama, M. Yoshida and Y. Norikane, *Chem.–Eur. J.*, 2013, **19**, 17391–17397.
- 24 Y. Norikane, E. Uchida, S. Tanaka, K. Fujiwara, E. Koyama, R. Azumi, H. Akiyama, H. Kihara and M. Yoshida, *Org. Lett.*, 2014, **16**, 5012–5015.
- 25 S. Wu, L. Niu, J. Shen, Q. Zhang and C. Bubeck, *Macromolecules*, 2009, **42**, 362–367.
- 26 G. Zou, H. Jiang, Q. Zhang, H. Kohn, T. Manaka and M. Iwamoto, *J. Mater. Chem.*, 2010, **20**, 285–291.
- 27 Q. Ye, X. You, G. Zou, X. Yu and Q. Zhang, *J. Mater. Chem.*, 2008, **18**, 2775–2780.
- 28 X. Chen, L. Hong, X. You, Y. Wang, G. Zou, W. Su and Q. Zhang, *Chem. Commun.*, 2009, 1356–1358.
- 29 H. Yamakoshi, K. Dodo, A. Palonpon, J. Ando, K. Fujita, S. Kawata and M. Sodeoka, *J. Am. Chem. Soc.*, 2012, **134**, 20681–20689.
- 30 A. Pal, P. Voudouris, M. M. E. Koenigs, P. Besenius, H. M. Wyss, V. Degirmenci and R. P. Sijbesma, *Soft Matter*, 2014, **10**, 952–956.
- 31 G. M. Sheldrick, *Acta Crystallogr., Sect. C: Struct. Chem.*, 2015, **71**, 3–8.
- 32 J. P. Perdew, K. Burke and M. Ernzerhof, *Phys. Rev. Lett.*, 1996, **77**, 3865–3868.
- 33 G. Kresse and J. Furthmuller, *Phys. Rev. B*, 1996, **54**, 11169–11186.
- 34 G. Kresse and D. Joubert, *Phys. Rev. B*, 1999, **59**, 1758–1775.
- 35 J. Algers, P. Sperr, W. Egger, L. Liskay, G. Kögel, J. de Baerdemaeker and F. H. J. Maurer, *Macromolecules*, 2004, **37**, 8035–8042.
- 36 J. G. Victor and J. M. Torkelson, *Macromolecules*, 1987, **20**, 2241–2250.
- 37 S. Xie, A. Natansohn and P. Rochon, *Chem. Mater.*, 1993, **5**, 403–411.
- 38 N. Liu, D. R. Dunphy, P. Atanassov, S. D. Bunge, Z. Chen, G. P. López, T. J. Boyle and C. J. Brinker, *Nano Lett.*, 2004, **4**, 551–554.
- 39 H. Bässler, V. Enkelmann and H. Sixl, *Polydiacetylenes*, Springer, Berlin, Heidelberg, Germany, 1984.
- 40 B. Yoon, S. Lee and J.-M. Kim, *Chem. Soc. Rev.*, 2009, **38**, 1958–1968.
- 41 B. Yoon, H. Shin, E.-M. Kang, D. W. Cho, K. Shin, H. Chung, C. W. Lee and J.-M. Kim, *ACS Appl. Mater. Interfaces*, 2013, **5**, 4527–4535.
- 42 R. W. Carpick, D. Y. Sasaki and A. R. Burns, *Langmuir*, 2000, **16**, 1270–1278.
- 43 J. Yoon, Y.-S. Jung and J.-M. Kim, *Adv. Funct. Mater.*, 2009, **19**, 209–214.
- 44 M. Irie, *Bull. Chem. Soc. Jpn.*, 2008, **81**, 917–926.
- 45 D. Zhitomirsky, E. Cho and J. C. Grossman, *Adv. Energy Mater.*, 2015, **6**, 1502006.
- 46 K. Ishiba, M.-a. Morikawa, C. Chikara, T. Yamada, K. Iwase, M. Kawakita and N. Kimizuka, *Angew. Chem., Int. Ed.*, 2015, **54**, 1532–1536.